C. R. Palevol 18 (2019) 223–235

Contents lists available at ScienceDirect

Comptes Rendus Palevol

www.sciencedirect.com

Human Palaeontology and Prehistory

The SKX 1084 hominin patella from Swartkrans Member 2, South Africa: An integrated analysis of its outer morphology and inner structure

La patelle hominine SKX 1084 du membre 2 de Swartkrans en Afrique du Sud : analyse intégrée de sa morphologie externe et de sa structure interne

Marine Cazenave[a,b,*], Anna Oettlé[a,c], John Francis Thackeray[d], Masato Nakatsukasa[e], Frikkie de Beer[f], Jakobus Hoffman[f], Roberto Macchiarelli[g,h]

[a] *Department of Anatomy, University of Pretoria, Pretoria, South Africa*
[b] *Computer-assisted Palaeoanthropology Team, UMR 5288 CNRS–Université Paul-Sabatier, 31000 Toulouse, France*
[c] *Department of Anatomy and Histology, Sefako Makgatho Health Sciences University, Ga-Rankuwa, Pretoria, South Africa*
[d] *Evolutionary Studies Institute and School of Geosciences, University of the Witwatersrand, Johannesburg, South Africa*
[e] *Laboratory of Physical Anthropology, Department of Zoology, Graduate School of Science, Kyoto University, Kyoto, Japan*
[f] *South African Nuclear Energy Corporation, Pelindaba, South Africa*
[g] *UMR 7194 CNRS–Muséum national d'histoire naturelle, Musée de l'Homme, 75013 Paris, France*
[h] *Unité de formation Géosciences, Université de Poitiers, 86073 Poitiers, France*

ARTICLE INFO

Article history:
Received 13 May 2018
Accepted after revision 28 June 2018
Available online 22 November 2018

Handled by Roberto Macchiarelli

Keywords:
Fossil hominins
Knee joint
Cortical bone
Cancellous network
X-ray micro-tomography

ABSTRACT

SKX 1084 is an isolated partial patella from Swartkrans Member 2, South Africa, attributed to a small-bodied *Paranthropus robustus*. This study provides complementary information on its outer conformation and, for the first time for a fossil hominin patella, documents its inner structure in the perspective of adding biomechanically-related evidence to clarify its identity. We used X-ray micro-tomography to investigate SKX 1084 and to extract homologous information from a sample of 12 recent human, one Neanderthal, and two adult *Pan*, patellae. We used geometric morphometrics to compare the outer equatorial contours. In SKX 1084, we identified two cancellous bony spots suitable for textural assessment (trabecular bone volume fraction, trabecular thickness, degree of anisotropy), and two related virtual slices for measuring the maximum cortico-trabecular thickness (CTT) of the articular surface. SKX 1084 shows a more complex articular shape than that for *Pan*, but still simpler than typical in *Homo sapiens*. At all sites, its CTT is thinner compared to *Pan* and approaches the condition in humans. This is also true for the expanded volume of the cancellous network. However, at both investigated spots, SKX 1084 is systematically intermediate between *Homo* and *Pan* for trabecular bone volume fraction and trabecular thickness, a pattern already shown in previous analyses on other *Paranthropus* postcranial remains. In the absence of any structural signal from patellae unambiguously sampling

* Corresponding author. Computer-assisted Palaeoanthropology Team, UMR 5288 CNRS–Université Paul-Sabatier, 31000 Toulouse, France.
E-mail address: marine.cazenave4@gmail.com (M. Cazenave).

https://doi.org/10.1016/j.crpv.2018.06.002

Paranthropus, as well as of comparable evidence extracted from specimens representing early *Homo*, our results do not allow rejection of the original taxonomic attribution of SKX 1084.

Mots clés :
Hominines fossiles
Articulation du genou
Os cortical
Réseau trabéculaire
Micro-tomographie à rayons X

RÉSUMÉ

SKX 1084 est une patelle isolée incomplète du membre 2 de Swartkrans, en Afrique du Sud, attribuée à un individu *Paranthropus robustus* de petite taille. La présente étude apporte des informations complémentaires sur sa conformation externe. Elle dévoile également, pour la première fois chez un hominine fossile, des caractéristiques de sa structure interne permettant d'extraire des informations biomécaniques pour clarifier son identité. Nous avons utilisé la microtomographie à rayons X pour étudier SKX 1084 et extraire des informations homologues à partir d'un échantillon composé de 12 patelles humaines récentes, un Néandertalien et deux chimpanzés, et appliqué la morphométrie géométrique pour comparer leurs contours externes. Nous avons identifié deux régions dans le tissu trabéculaire de SKX 1084, qui sont adaptées à l'évaluation texturale (densité osseuse, épaisseur trabéculaire, degré d'anisotropie), et nous avons extrait deux coupes virtuelles pour mesurer l'épaisseur cortico-trabéculaire maximale (CTT) de la surface articulaire. SKX 1084 présente une forme articulaire plus complexe que celle des chimpanzés, mais plus simple que celle d'*Homo sapiens*. Son CTT est partout moins épais par rapport à *Pan* et se rapproche de la condition humaine. Ceci est également vrai pour le volume global du réseau trabéculaire. Cependant, pour les deux régions étudiées, SKX 1084 montre une densité osseuse et une épaisseur trabéculaire intermédiaire entre *Homo* et *Pan*, une tendance déjà observée dans de précédentes analyses d'autres restes postcrâniens de *Paranthropus*. En l'absence de toute information quant au signal structural d'autres patelles de *Paranthropus* ainsi que d'éléments comparables issus des premiers représentants du genre *Homo*, nos résultats ne permettent pas de rejeter l'attribution taxonomique originale de SKX 1084.

1. Introduction

The discovery of isolated fragmentary hominin remains from the axial and appendicular skeleton in the Plio-Pleistocene South African cave deposits is a rather frequent occurrence that complicates the task of confidently assessing diversity in contexts where *Australopithecus*, *Paranthropus* and early *Homo* may have co-existed (Berger et al., 2010; Braga et al., 2016; Cazenave et al., 2017; Grine and Susman, 1991; Keyser et al., 2000; Lague, 2015; McHenry, 1975; McHenry et al., 2007; Moggi-Cecchi et al., 2010; Schwartz and Tattersall, 2003; Susman and Brain, 1988; Susman and de Ruiter, 2004; Susman et al., 2001). An example of such difficulties is represented by the specimen SKX 1084, an isolated partial patellar bone from Swartkrans Member 2 commonly attributed to a small-bodied *P. robustus* individual (Susman, 1988, 1989). However, the estimated chronology of Swartkrans Member 2 (1.36–1.1 Ma) (Balter et al., 2008; Delson, 1988; Gibbon et al., 2014; Herries et al., 2009; Vrba, 1975) is also compatible with the presence in the area of representatives of the genus *Homo*, whose percentage in the Swartkrans Members 1–3 hominin assemblage has been estimated to 9% (Pickering et al., 2012).

Rare Pliocene–early Pleistocene hominin patellar specimens are usually reported for their size and outer gross morphology (e.g. Alemseged et al., 2006; Carretero et al., 1999; DeSilva et al., 2013; Harrison and Kweka, 2011; Lordkipanidze et al., 2007; Martín-Francés et al., 2016). However, given the topographic context of the hominin knee joint (Aiello and Dean, 1990; Lovejoy, 2007) and the documented ability of bone tissues to adjust structurally to the loading environments (e.g. Carlson and Marchi, 2014; Gosman et al., 2011; Kivell, 2016; Lieberman et al., 2004; Pearson and Lieberman, 2004; Ruff et al., 2006; Wallace et al., 2012), the so far unexplored combined signals from the outer and the inner patellar structure have the potential to provide subtle functionally-related information. Indeed, the differences between the human and ape knee joint configurations are part of a suite of traits intimately related to habitual postural and locomotion modes (e.g. Aiello and Dean, 1990; Frelat et al., 2017; Lovejoy, 2007; Mazurier et al., 2010; Sylvester, 2013; Tardieu, 1999; Zipfel and Berger, 2009). With regard to the patella, such differences do not only concern its outer proportions and shape and the extension and insertion topography of the quadriceps complex (smaller in the latter, where flexion prevails) and of the vastus medialis (which in apes does not insert onto its extreme medial edge) (Aiello and Dean, 1990; Lovejoy, 2007; Mariani et al., 1978; Masouros et al., 2010; Standring, 2008; Taylor et al., 2004), but should also be expressed in terms of regional variation of the patellar subchondral bone thickness and structural arrangement of the underlying cancellous network (for the human patella, see Katoh

Fig. 1. The left patella SKX 1084 from Swartkrans, South Africa, in anterior (a) and posterior (b) views. Scale bar: 10 mm.
Fig. 1. La patelle gauche SKX 1084 de Swartkrans, en Afrique du Sud, en vues antérieure (a) et postérieure (b). Barre d'échelle : 10 mm.

et al., 1996; Raux et al., 1975; Toumi et al., 2006, 2012; Touraine et al., 2017; Townsend et al., 1975, 1977).

Following Kivell, (2016: 587) "variation in trabecular structure is our best source of morphological information that is preserved in the fossil record, particularly when analysed in conjunction with cortical bone, for reconstructing actual, rather than potential, behaviours in fossil hominoids and hominins". However, while the outer aspect of SKX 1084 has been the object of description and comparative morphological analysis (Ramirez and Pontzer, 2015; Susman, 1988, 1989; Susman et al., 2001), its inner structural organization remains unreported (Cazenave et al., 2016).

By assuming that the patella bears a functionally-related signal and that the *Paranthropus* inner structural signature should be somehow distinct from the human one (for the proximal femur, for example, see Chirchir et al., 2015; Ryan et al., 2018), in this exploratory study we use imaging techniques applied to an X-ray micro-tomographic record of SKX 1084 (i) to integrate and comparatively assess its outer conformation and (ii) to detail and preliminarily compare its inner characteristics to homologous features extracted from a recent human sample, a Neanderthal individual and two *Pan* representatives. Given the current lack of similar combined information extracted from the patellar bone of any pre-modern human and extant and fossil non-human hominid, the present exploratory study represents a first qualitative and quantitative three-dimensional (3D) glimpse useful for the future assessment of isolated hominin patellar remains.

2. Materials and methods

2.1. Materials

SKX 1084 represents the superior two-thirds of an undistorted, relatively well-preserved while incomplete left patella (Fig. 1). Its ossification, general morphology and the degree of development of some longitudinal markings on its anterior surface (likely related to the quadriceps tendon) indicate it comes from an adult individual, even if surface rugosity may have been locally accentuated by mineral matrix dissolution. The specimen preserves the entire base, which slopes antero-inferiorly from behind; however, its cortical shell is chipped all along the superior posterior margin, approximately at the insertion of the vastus intermedius tendon, thus revealing an underlying trabecular network partially filled by sediment. The lateral border is nearly intact, but the specimen lacks the apex and almost entirely its medial border, uniquely represented by its uppermost portion. Posteriorly, the articular portion which contacts the lateral lip of the femoral trochlea is virtually intact. As a whole, this specimen shows an only modest degree of mineralization. While its maximum height cannot be assessed, SKX 1084 has a medio-lateral breadth of 30.2 mm (Susman, 1989) and an antero-posterior thickness near its centre of 13.0 mm (original measure).

SKX 1084 was previously curated at the Ditsong National Museum of Natural History, Pretoria. Since 2016 the specimen has been integrated into the fossil hominin collections of the Evolutionary Studies Institute at the University of the Witwatersrand, Johannesburg.

The comparative material used in this study consists of human and chimpanzee adult patellae, all lacking macroscopic evidence of alteration or pathological change. The recent human specimens come from six individuals of African ancestry (4 males and 2 females aged 24–29 years) selected from the Pretoria Bone Collection at the Department of Anatomy of the University of Pretoria (L'Abbé et al., 2005), and from six individuals (2 likely males and 4 likely females whose estimated age at death ranges between 30 and 50 years) from the Imperial Roman graveyard of Velia, Italy, stored at the National Prehistoric Museum of Rome (review in Beauchesne and Agarwal, 2017). The fossil human representative is the perfectly preserved left patella from the OIS 4 Neanderthal partial skeleton Regourdou 1, from the homologous rock shelter in Dordogne, France, stored at the "Musée d'art et d'archéologie du Périgord, Périgueux" (Bayle et al., 2011; Maureille et al., 2015). We also studied two female chimpanzee patellae from the

Mahale skeletal collection stored at the Japan Monkey Centre of Inuyama, Japan.

2.2. Methods

All specimens were imaged by X-ray microtomography. SKX 1084 was scanned in 2015 at the South African Nuclear Energy Corporation (Necsa), Pelindaba, using a Nikon XTH 225 ST equipment with an isotropic voxel size of 16.2 μm. The human patellae from the Pretoria Bone Collection were also recorded at Necsa, in 2016, with an isotropic voxel size ranging from 24.0 μm to 29.0 μm, while the archaeological specimens from Velia were scanned in 2012 at the Multidisciplinary Laboratory of the International Centre for Theoretical Physics (ICTP) of Trieste, Italy (Tuniz et al., 2013), at an isotropic voxel size ranging from 26.5 μm to 33.1 μm. The Neanderthal Regourdou 1 was imaged in 2004 by SR-μCT at the beamline ID 17 of the European Synchrotron Radiation Facility (ESRF) of Grenoble, France, at an isotropic spatial resolution of 45.5 μm (Bayle et al., 2011). Finally, the two chimpanzee patellae were recorded in 2017 at the Laboratory of Physical Anthropology, Kyoto University, using a ScanXmate A080s (Comscan co.) equipment with an isotropic voxel size of 48.5 μm. Following acquisition, a virtual transformation of each dataset was necessary to coherently orient the specimens by using Avizo© v.8.0.0. (Visualization Sciences Group Inc.).

The articular (posterior) surface of the patella presents distinct differences in extant and extinct hominids (Aiello and Dean, 1990; Lovejoy, 2007; Masouros et al., 2010; Pina et al., 2014; Pritchard, 1980; Standring, 2008; Ward et al., 1995; for a review, see Pina, 2016). Accordingly, before detailing its inner structure, we virtually extracted the transverse section of SKX 1084 at its maximum medio-lateral breadth and performed a comparative geometric morphometric (GM) analysis of its unsmoothed outer equatorial contour with respect to the outlines extracted from the comparative material used in this study. However, because of local bony discontinuities on the anterior surface of the South African specimen (Fig. 1), the anterior portion of its cross-section was reconstructed by two independent observers by using the preserved contours of the antero-lateral and medial regions as a guide. Accordingly, three outer outlines of SKX 1084 displaying an increasing degree of anterior convexity were generated (see Supporting information, Fig. S1). On each virtually reconstructed outline (a to c), 100 semilandmarks were placed following the sectional contour using the B-spline module in Avizo© v.8.0.0. Using the package Morpho v.2.5.1 (Schlager, 2017) for R v.3.4.0 (R Development Core Team, 2017), a generalized Procrustes analysis (GPA) and a weighted between-group principal component analysis (bgPCA) based on the Procrustes shape residuals (Mitteroecker and Bookstein, 2011) were then performed to compare the three reconstructed versions of SKX 1084 and the human and chimpanzee shapes. Allometry was tested on the landmark-based analyses using the coefficient of determination (R^2) of a multiple regression (Bookstein, 1991), in which the explicative variable is the centroid size and the dependent variables are the bgPC scores (Mitteroecker et al., 2013).

Relatively well preserved cancellous network spots in SKX 1084 were found in the central and medial posterior areas; however, the amount of cemented matrix infill permeating the network increased towards its outer surface, especially laterally and anteriorly. Accordingly, we firstly identified in the inner central and medial upper portion of SKX 1084 two cubic volumes of interest (Ryan and Ketcham, 2002a, 2002b), aVOI and bVOI, respectively, suitable for textural properties assessment (Fig. 2). Both had an edge length equal to 11% of the medio-lateral breadth (i.e. 3.32 mm in SKX 1084, which corresponds to a volume of 36.6 mm^3). The centre of aVOI was placed midway between 50% of the medio-lateral diameter and its most distant point on the upper margin along an axis perpendicular to the breadth. The bVOI was positioned medially to the aVOI, the distance between the two centres corresponding to 25% of the medio-lateral diameter (i.e. 7.6 mm in SKX 1084). The same analytical protocol was systematically applied to the specimens used for comparison. In extant humans the VOIs range in size from 70.2 mm^3 to 151.9 mm^3 and from 13.8 mm^3 to 15.6 mm^3 in *Pan*.

At two sites of the articular surface topographically related to the VOIs defined above, we measured the maximum thickness of the cortico-trabecular complex (CTC, in mm), i.e. the subchondral component which includes the cortical shell (lamina) and the intimately related adjoining portions of the supporting trabecular network, which mostly consists of plate-like structures (Supporting information, Fig. S2; Beaudet et al., 2013; Mazurier, 2006; Mazurier et al., 2006, 2010; Volpato, 2007). The maximum cortico-trabecular thickness (CTT) was measured by the routine MPSAKv2.9© (in Dean and Wood, 2003) on two sagittal virtual slices set perpendicular to the posterior face of each VOI and crossing their centre (Fig. 2). To facilitate comparisons, in each specimen such measures (aCTT and bCTT) were standardized with respect to the medio-lateral diameter of the patella. Unfortunately, in SKX 1084 we could not similarly assess the anterior CTT, as in this specimen the cortical shell was not preserved and some matrix infill obscured the boundaries.

The cubic VOIs were binarized into bone and non-bone using the "Half Maximum Height" (HMH) quantitative iterative thresholding method (Spoor et al., 1993) and the region of interest protocol (ROI-Tb; Fajardo et al., 2002) by taking repeated measurements on different slices of the virtual stack (Coleman and Colbert, 2007) using Avizo© v.8.0.0. and ImageJ© (Schneider et al., 2012). Because of local matrix infill, segmentation of the specimen SKX 1084 required manual interventions. By using the star volume distribution (SVD) algorithm in Quant3D© (Ryan and Ketcham, 2002a, b), on each virtually extracted VOI we measured the following variables:

- the trabecular bone volume fraction (BV/TV, in %), given as the ratio of the number of bone voxels to the total number of voxels;
- the trabecular thickness (Tb.Th., in mm), which is the mean thickness of the trabecular struts;

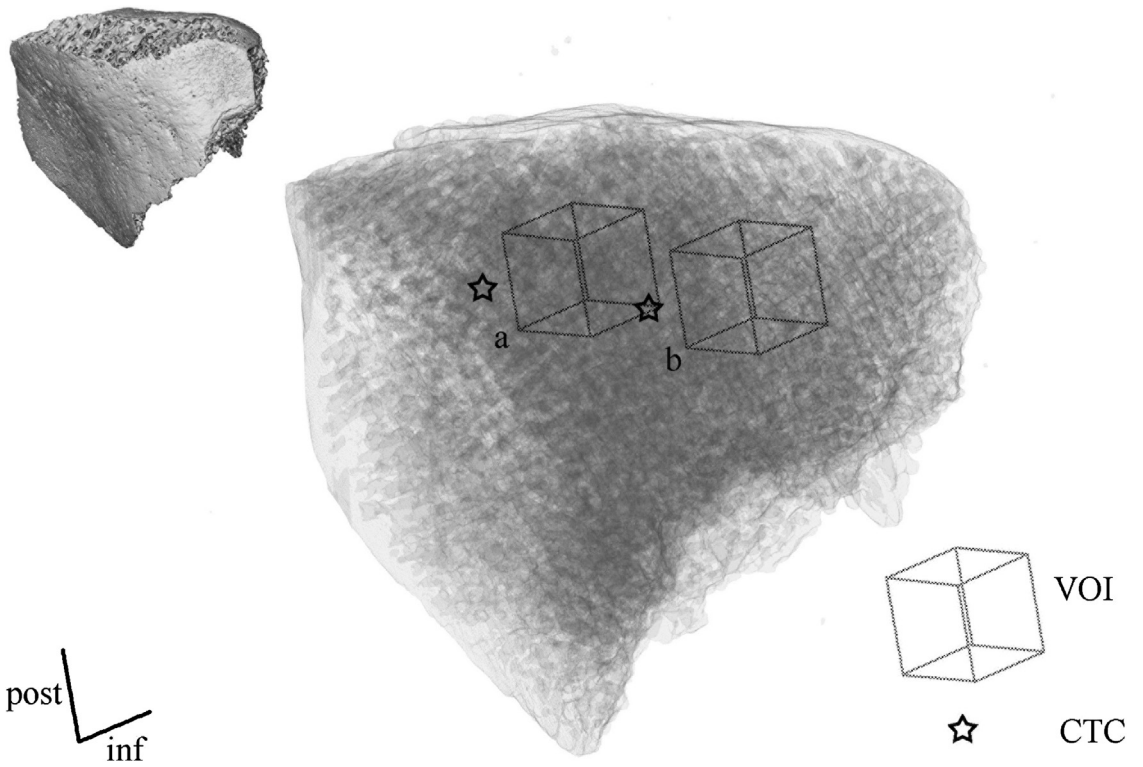

Fig. 2. 3D tomographic oblique posterior view of SKX 1084 in semi-transparency showing the position of the central (a) and medial (b) cubic volumes of interest (VOI) extracted for assessing cancellous bone properties and the two topographically related slices (aCTC and bCTC) sampling the cortico-trabecular complex of the articular surface. The virtual reconstruction of the outer surface of the specimen (not to scale) is only provided for orientation.
Fig. 2. Rendu 3D virtuel en vue postérieure oblique de SKX 1084, montrant par semi-transparence la position des volumes cubiques d'intérêt (VOI) central (a) et médial (b) extraits pour analyser les propriétés de l'os trabéculaire et les deux coupes topographiquement liées (aCTT et bCTT) échantillonnant le complexe cortico-trabéculaire de la surface articulaire. La reconstruction virtuelle de la surface externe du spécimen (pas à l'échelle) est simplement donnée pour orientation.

- and the degree of anisotropy (DA), a fabric characteristic of trabecular bone assessed following Ryan and Ketcham (2002a; see also Ryan and Walker, 2010; Shaw and Ryan, 2012) by dividing the eigenvalue representing the relative magnitude of the primary material axe of the bone structure (τ_1) by the eigenvalue representing the relative magnitude of the tertiary material axe of the bone structure (τ_3).

For all variables, a number of intra- and inter-observer tests for accuracy run by three independent observers revealed differences less or equal to 5%.

3. Results

For the medio-lateral breadth and the antero-posterior thickness, SKX 1084 fits the proportions shown by *H. floresiensis* (Jungers et al., 2009) and *A. sediba* (DeSilva et al., 2013), and also approaches those of the slightly thicker *H. naledi* (Berger et al., 2015; Marchi et al., 2017) and the slightly smaller male and female chimpanzee patellae (Aiello and Dean, 1990; Pina, 2016; Pina et al., 2014; Pritchard, 1980; Ward et al., 1995). Conversely, SKX 1084 is systematically smaller compared to *H. erectus* (*georgicus*) from Dmanisi (Lordkipanidze et al., 2007; T. Jashawili, pers. comm.), *H. antecessor* (Carretero et al., 2001), the Neanderthals (Radovčić et al., 1988; Trinkaus, 1983; Vandermeersch, 1981; and original data), as well as to the extant human figures (Baldwin and House, 2005; Dayal and Bidmos, 2005; Iranpour et al., 2008; Kemkes-Grottenthaler, 2005; Olateju et al., 2013; Yoo et al., 2007) (Fig. 3 and Supporting Information, Table S1).

The bgPCA based on the Procrustes shape coordinates of the three reconstructed outer outlines of the transverse section at the maximum medio-lateral breadth of SKX 1084 (a to c; see Supporting information, Fig. S1) are shown in Fig. 4 together with those of the human and chimpanzee specimens. The first two components (bgPC1 and bgPC2) show no allometric signal ($R^2 = 0.02$) and no size-dependent shape variation ($R^2 = 0.01$). In the analysis, the three reconstructed equatorial profiles of the South African fossil patella cluster together and are distinct from both the human and chimpanzee morphotypes. Specifically, by showing a proportionally more ovoid outline, SKX 1084 and the two *Pan* used in this analysis fall in the negative space of bgPC1, whereas all human specimens, including the Neanderthal Regourdou 1, are mostly found in the positive space of bgPC1 because of their more complex articular shape showing concave articular facets and a convex vertical ridge. The three contours of SKX 1084 and the two *Pan*

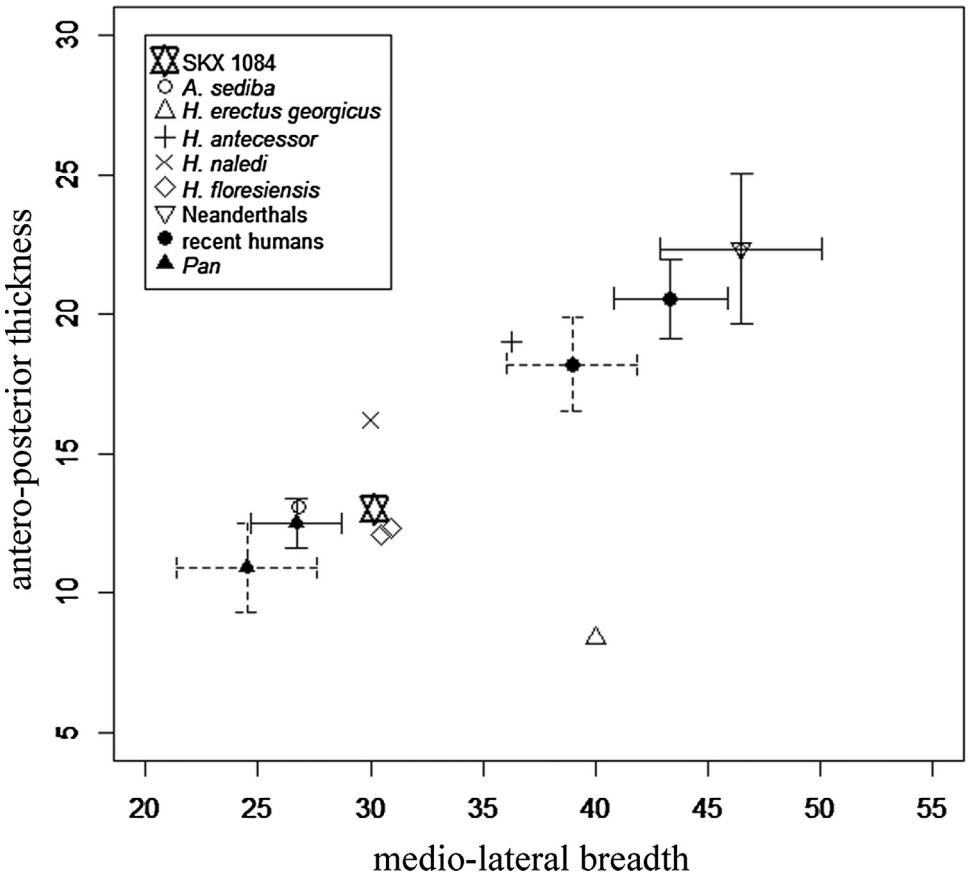

Fig. 3. Medio-lateral breadth and antero-posterior thickness of SKX 1084 compared to those of *Australopithecus sediba* (DeSilva et al., 2013), *Homo erectus georgicus* (Lordkipanidze et al., 2007; T. Jashawili, pers. comm.), *H. antecessor* (Carretero et al., 2001), *H. naledi* (Berger et al., 2015; Marchi et al., 2017), *H. floresiensis* (Jungers et al., 2009), Neanderthals ($n = 12$; pooled specimens from Krapina: Radovčić et al., 1988 and original data; Regourdou 1, Tabun 1, La Ferassie 2, La Chapelle-aux-Saints, Spy II: Vandermeersch, 1981 and original data; Shanidar: Trinkaus, 1983), recent humans ($n = 60$ males and 60 females; Dayal and Bidmos, 2005), *Pan* ($n = 14$ males and 20 females; Pritchard, 1980). For the Neanderthal, recent human and *Pan* samples, the average value ± 1 s.d. is shown; in the human and *Pan* samples, the dashed lines correspond to the female, that continuous to the male estimates.

Fig. 3. Largeur médio-latérale et épaisseur antéro-postérieure de SKX 1084 par rapport à celles d'*Australopithecus sediba* (DeSilva et al., 2013), *Homo erectus georgicus* (Lordkipanidze et al., 2007 ; T. Jashawili, comm. pers.), *H. antecessor* (Carretero et al., 2001), *H. naledi* (Berger et al., 2015 ; Marchi et al., 2017), *H. floresiensis* (Jungers et al., 2009), Néandertaliens ($n = 12$; spécimens de Krapina : Radovčić et al., 1988 et données originales ; Regourdou 1, Tabun 1, La Ferassie 2, La Chapelle, Spy II : Vandermeersch, 1981 et données originales ; Shanidar : Trinkaus, 1983), humains récents ($n = 60$ hommes and 60 femmes ; Dayal and Bidmos, 2005), *Pan* ($n = 14$ mâles and 20 femelles ; Pritchard, 1980). Pour les échantillons des Néandertaliens, des humains récents et des chimpanzés, la valeur moyenne ± 1 d.s. est donnée. Pour les humains et les chimpanzés, la ligne en pointillés correspond aux estimations concernant les femelles et celle en continu aux estimations concernant les mâles.

representatives were discriminated along bgPC2, the fossil specimen exhibiting a more rounded shape compared to the flatter chimpanzee shape (Fig. 4).

In terms of volume and spatial organization, the cancellous network preserved in SKX 1084 is globally closer to the human than to the *Pan* condition, even if in coronal view the specimen from Swartkrans and *Pan* show a slightly more honeycomb-like, vacuolar appearance of the cancelli in respect to the human pattern (Fig. 5). Specifically, despite its incompleteness, SKX 1084 shares with humans a larger proportional volume of trabecular bone compared to *Pan*, a denser area at the supero-lateral margin (likely related to the attachment of the quadriceps), and a higher number of radially oriented trabeculae at the medial and superior peripheral areas. In sagittal view, a typically human vertically oriented anterior bundle (Standring, 2008), also appreciable in transversal view, is noticeable in SKX 1084 (where it is anyhow incompletely preserved inferiorly), while *Pan* displays at all sites a relatively and absolutely thicker cortical shell and much less expanded but denser spongy bone.

For both relative (%) values of the maximum cortico-trabecular thickness (CTT) measured at the central (aCTT) and medial (bCTT) spots of the posterior surface (Fig. 6), SKX 1084 fits the recent human estimates and is distinct from the thicker *Pan* condition (Table 1). In this context, the proportionally thinnest cortico-trabecular complex was found at the bVOI of the Regourdou 1 Neanderthal specimen.

As measured in both central and medial VOIs (Table 2), SKX 1084 shows a relative bone volume fraction (BV/TV) intermediate between the human and the chimpanzee estimates, *Pan* being over twice denser than observed in all human specimens used in this study, including the

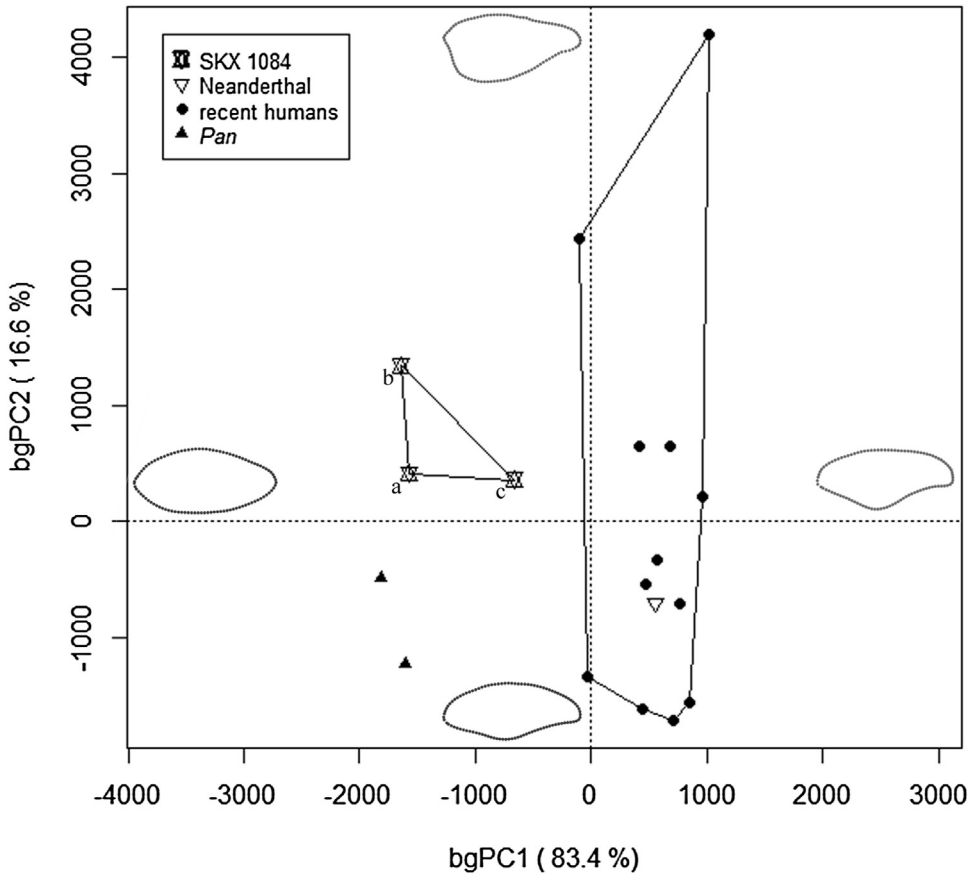

Fig. 4. Between-group principal component analysis (bgPCA) of the Procrustes shape coordinates of the three reconstructions of the outer outline of the transverse section across the maximum medio-lateral breadth of SKX 1084 (a, b, c), a Neanderthal (Regourdou 1), recent humans ($n = 12$), and *Pan* ($n = 2$).
Fig. 4. Analyse en composantes principales intergroupe, réalisée à partir des coordonnées Procuste de trois reconstructions du contour externe de la section transversale extraite au niveau de la largeur médio-latérale maximale de SKX 1084 (a, b, c) comparées à un Néandertalien (Regourdou 1), des humains récents ($n = 12$) et *Pan* ($n = 2$).

Table 1
Maximum thickness of the cortico-trabecular complex (in mm) standardized by the medio-lateral breadth of the patella (% values) measured from the articular surface in correspondence of the central (aCTT) and medial (bCTT) volumes of interest (see Fig. 2) in SKX 1084, recent humans ($n = 12$), a Neanderthal (Regourdou 1), and *Pan* ($n = 2$); s.d., standard deviation.
Tableau 1
Épaisseur maximale du complexe cortico-trabéculaire (en mm), standardisée par la largeur médio-latérale de la patella (%) mesurée à partir de la surface articulaire en correspondance avec les volumes d'intérêt central (aCTT) et médial (bCTT) (voir Fig. 2) pour SKX 1084, les humains récents ($n = 12$), un Néandertalien (Regourdou 1) et *Pan* ($n = 2$) ; s.d., déviation standard.

Specimens/samples	aCTT (%)	bCTT (%)
SKX 1084	9.6	7.2
Recent humans(s.d.)	8.7 (1.4)	7.1 (1.7)
Neanderthal	8.0	4.6
Pan	12.4–12.7	9.3–10.8

Neanderthal representative. An intermediate position is again shown by SKX 1084 for the average trabecular thickness (Tb.Th.), all humans systematically displaying thinner struts. For the degree of anisotropy (DA), the South African fossil specimen closely fits the modern human estimates for the central aVOI, while for the medial bVOI it is intermediate between the higher human values and the generalized lower degree of anisotropy displayed by the chimpanzee patella. Interestingly, for all variables considered here, the Neanderthal specimen always falls within the extant human range, which is not the case for SKX 1084 but for the DA of the aVOI (Table 2).

4. Discussion

This exploratory study aimed at tentatively adding previously unreported biomechanically-related evidence to clarify the common allocation of the SKX 1084 patella from Swartkrans to the taxon *Paranthropus* (e.g. Jungers, 1988; Marchi et al., 2017; McHenry, 1991; Ramirez and Pontzer, 2015; Susman, 1988, 1989, 2004; Susman and Brain, 1988; Susman and de Ruiter, 2004; Susman et al., 2001; Sylvester et al., 2011). Besides the incomplete preservation of this specimen and its limited amount of subchondral and cancellous bone spots preserved for reliable quantitative assessment, the major limiting factor in this study is the lack of comparative information on the inner structural organization characterizing any nonhuman fossil hominin patella (including in *Australopithecus*) and, of course, that of any specimen confidently representing early *Homo*.

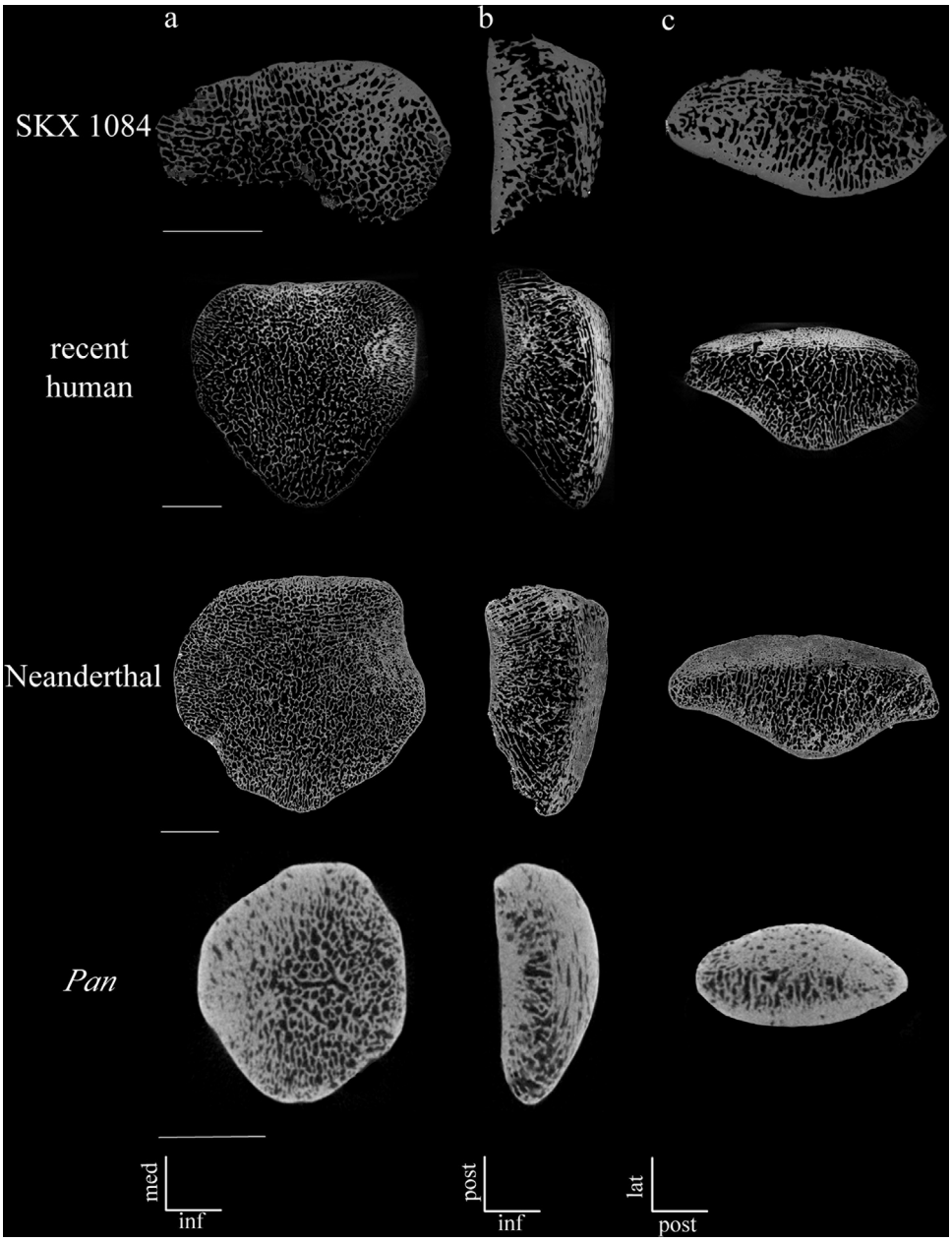

Fig. 5. Coronal (a), parasagittal (b) and transversal (c) virtual sections from 3D tomographic view approximately across the centre of the patella in SKX 1084, a recent human (male, 26 years old), a Neanderthal (Regourdou 1), and a female chimpanzee (M09). Scale bars: 10 mm.
Fig. 5. Sections virtuelles coronale (a), parasagittale (b) et transversale (c) extraites à partir de vues tomographiques 3D approximativement au centre de la patelle SKX 1084, d'un humain récent (homme, 26 ans), d'un Néandertalien (Regourdou 1) et d'une femelle chimpanzé (M09). Barre d'échelle : 10 mm.

Nonetheless, we consider that some results obtained from the present analyses may deserve attention in similar future studies.

Ramirez and Pontzer (2015) have suggested that patellar dimensions can be used in extant primate and fossil hominin taxa as proxy for the physiological cross-sectional area of the quadriceps, the primary extensor of the knee (see also Pina et al., 2014; Trinkaus, 1983, and the review in Pina, 2016). While the maximum height cannot be measured in SKX 1084, its medio-lateral breadth and antero-posterior thickness fit the dimensions of diminutive *H. floresiensis* and of *A. sediba*, and more closely approach those of *Pan* and *H. naledi* than the size of any other human patella reported so far. The patellar antero-posterior thickness and supero-inferior height (the latter unknown in SKX 1084), but not the medio-lateral breadth, appear to play a major role in the length of the patellar tendon moment arm and in the lever arm length associated with the quadriceps, respectively (Pina, 2016; Pina et al., 2014; Ward et al., 1995). Accordingly, whenever the conclusions by Ramirez

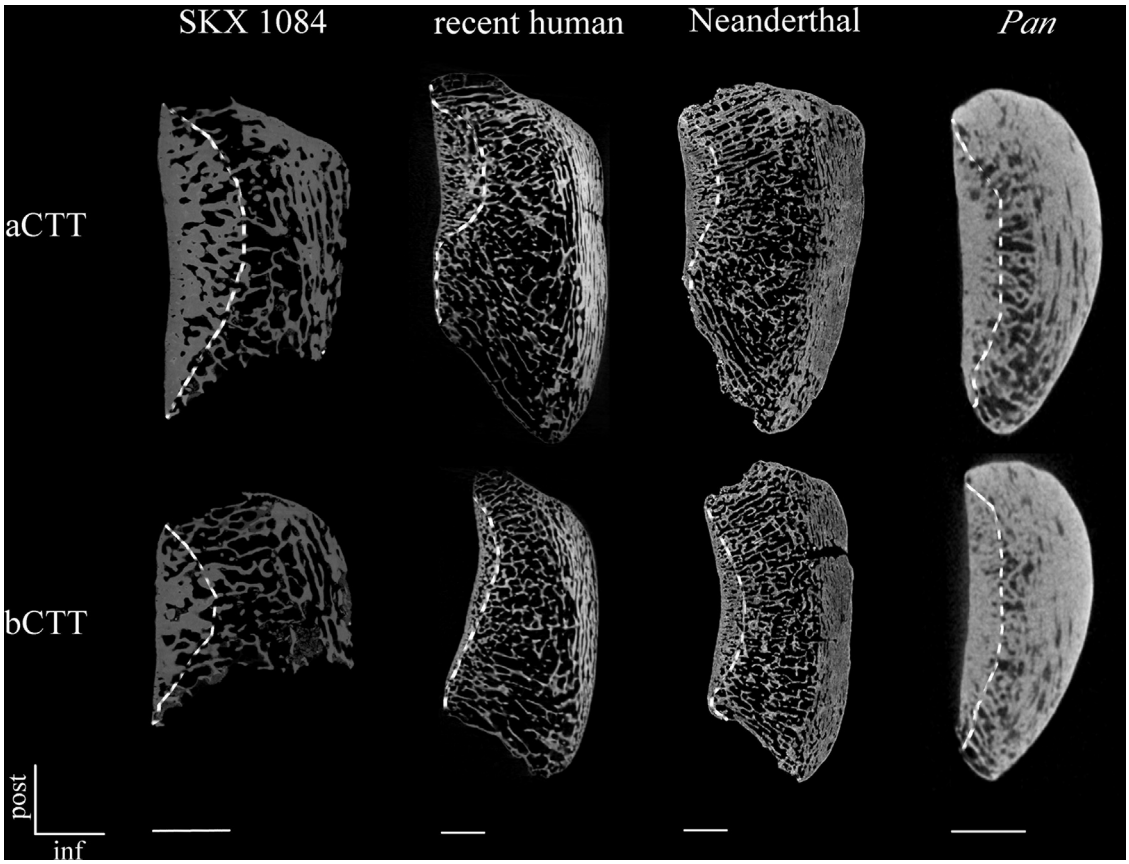

Fig. 6. Transversal sections across the central (aVOI) and medial (bVOI) 3D tomographic volumes of interest of the patella (see Fig. 2) in SKX 1084, a recent human (male, 26 years old), a Neanderthal (Regourdou 1), and a female chimpanzee (M09); in each section, the dashed line delimits the cortico-trabecular complex measured for its maximum thickness (aCTT and bCTT, respectively) from the articular surface. Scale bars: 5 mm.
Fig. 6. Sections transversales extraites au centre des volumes d'intérêts central (aVOI) et médial (bVOI) de la patelle (voir Fig. 2) de SKX 1084, d'un humain récent (homme, 26 ans), d'un Néandertalien (Regourdou 1) et d'une femelle chimpanzé (M09). Pour chaque section, la ligne en pointillés délimite le complexe cortico-trabéculaire mesuré pour son épaisseur maximale (respectivement, aCTT et bCTT) au niveau de la surface articulaire. Barre d'échelle : 5 mm.

and Pontzer (2015) are correct, the relatively small-sized fossil hominin patellae considered here, including SKX 1084 (Fig. 3 and Supporting information, Table S1), should represent taxa having experienced a limited home range size compared to that expected for *Homo* (Antón, 2013; Antón et al., 2014; Ramirez and Pontzer, 2015).

Comparative research on structural anatomy and functional morphology supports the view that the mammalian knee is an especially complex joint (Lovejoy, 2007: 326), including in primates, where shape variation of the patellar articular surface plays a key functional role. In humans, where the patella tends to have the thickest articular cartilage in the entire body (Masouros et al., 2010; Standring, 2008), its smaller medial facet contacts the antero-lateral portion of the medial femoral condyle and the wider lateral facet contacts the anterior part of the lateral condyle only in full flexion, while in extension the patellar-femoral contact is limited to the lowest portions of both facets (Aglietti and Menchetti, 1995; Goodfellow et al., 1976; Lovejoy, 2007; Pina, 2016). Compared to the multifaceted human patella bearing several distinctly angulated planes, a simpler articular morphology is found in *Pan*, where the posterior surface is relatively smooth and casts the similarly flatter trochlear surface (patellar groove) of the distal femur (Aiello and Dean, 1990; Lovejoy, 2007). With this respect, while necessarily limited to the equatorial contour, our GM-based shape analysis confirms such distinction in articular complexity between *Homo* and *Pan* and also reveals that the SKX 1084 outline occupies a somehow intermediate morphospace. Additional research work is needed to relate such differences in the outer conformation of the hominid patellar bone to locomotion-related differences in knee joint kinematics.

Especially when assessed in fossil remains, the inner boundaries of the so-called cortico-trabecular complex (CTC) are locally difficult to define (e.g. Mazurier, 2006; Mazurier et al., 2006, 2010; Volpato, 2007; Supporting information, Fig. S2). Nonetheless, compared to the human condition, the chimpanzee patella unambiguously shows at all sites a relatively thicker and denser CTC, notably expressed by a distinctly thicker anterior lamina which, in both individuals used in this study, is about twofold as thick as measured in our human comparative sample (Supporting information, Fig. S3 and Table S2).

Table 2
Bone volume fraction (BV/TV, in %), trabecular thickness (Tb.Th., in mm), and degree of anisotropy (DA) of the central (aVOI) and medial (bVOI) volumes of interest of the patella (see Fig. 2) assessed in SKX 1084, recent humans ($n = 12$), a Neanderthal (Regourdou 1), and *Pan* ($n = 2$); s.d., standard deviation.
Tableau 2
Volume osseux (BV/TV, en %), épaisseur trabéculaire (Tb.Th., en mm) et degré d'anisotropie (DA) des volumes d'intérêt central (aVOI) et médial (bVOI) de la patelle (voir Fig. 2) mesurée pour SKX 1084, les humains récents ($n = 12$), un Néandertalien (Regourdou 1) et *Pan* ($n = 2$) ; s.d., déviation standard.

Specimens/samples	aVOI			bVOI		
	BV/TV (%)	Tb.Th. (mm)	DA	BV/TV (%)	Tb.Th. (mm)	DA
SKX 1084	40.4	0.20	3.83	38.6	0.19	2.73
Recent humans(s.d.)	30.5 (6.5)	0.15 (0.03)	3.87(1.46)	26.5 (5.7)	0.14 (0.03)	4.92(1.52)
Neanderthal	34.5	0.15	4.44	30.3	0.13	5.81
Pan	65.1–79.1	0.23–0.27	2.73–2.87	67.8–81.2	0.23–0.24	1.88–1.94

Interestingly, relatively and absolutely higher values of cortico-trabecular thickness in *Pan* are also found at both medial and lateral condyles of the tibial plateau compared to the human condition (Mazurier, 2006; Mazurier et al., 2010). In the small-sized chimpanzee patella, this greater proportional amount of subchondral bone is associated with a relatively and absolutely reduced volume of vacuolar spongy bone. To the contrary, the human patella displays a proportionally thinner shell and a relatively and absolutely higher volume of locally more structured cancellous bone, thus behaving as a kind of "sandwich" construction combining high strength with relatively low density (Dalstra and Huiskes, 1995; Huiskes, 2000). As subchondral bone tends to respond to loading of the complementary joint surface, while cancellous bone primarily responds to forces travelling through the bone itself (Su, 2011; Zeininger et al., 2011), the gross structural solutions distinguishing the human and chimpanzee patellae reflect two ways of dealing with different patterns of mechanical stresses at the joint, those acting on the human patella being greater medially and centrally than laterally (Toumi et al., 2006, 2012). With this respect, while cortico-trabecular thickness variation across the anterior surface cannot be assessed in SKX 1084, thickness measured at two sites beneath its articular surface fits the human figures, as also does its proportion of spongy bone.

In terms of textural properties assessed at two cancellous volumes of interest selected because of the quality of their signal, our results show that, apart from a relatively honeycomb-like appearance and a slightly less structured medial aspect, the inner organization of SKX 1084 more closely resembles the human than the *Pan* condition. Whereas SKX 1084 displays a denser cancellous network and relatively thicker struts than measured in our recent human sample and in the Neanderthal representative, the South African fossil specimen and humans are more gracile compared to *Pan*.

According to recent interpretations based on the comparative analysis of the cancellous network properties assessed in the femoral head of extinct and extant hominids, humans and australopiths share a higher degree of anisotropy than typical in extant apes as response to the more stereotypic loading conditions at the hip joint imposed by habitual bipedal locomotion (Ryan et al., 2018). Similarly, the distinctly human-like signal from at least the more centrally-placed aVOI detected in this study in SKX 1084, which is higher than measured in *Pan*, is compatible with the model of a limited range of habitual knee joint motion, i.e. with a human-like gait kinematics. However, given the limited number of cases investigated so far, this hypothesis remains to be tested on more representative hominid samples.

A number of studies having investigated the structural features in some postcranial hominin remains show that, compared to the typically human figures (e.g. Chirchir et al., 2015, 2017; Ryan and Shaw, 2015), *Paranthropus* commonly possesses a thicker cortex and a denser, thicker and less anisotropic cancellous network, but also that its conformation is globally closer to the human than to the ape pattern (Bleuze, 2010; Cazenave et al., 2017; Chirchir et al., 2015; DeSilva and Devlin, 2012; Domínguez-Rodrigo et al., 2013; Dowdeswell et al., 2016; Macchiarelli et al., 1999, 2001; Ruff and Higgins, 2013; Ruff et al., 1999; Ryan et al., 2018; Skinner et al., 2015; Su and Carlson, 2017; Su et al., 2013). With this respect, as the condition characterizing early *Homo* is still unknown, the endostructural signal preserved in SKX 1084 is compatible with what is expected for *Paranthropus*. However, depending on the investigated regions, more human- or chimpanzee-like textural features have been observed at site-specific level in both *Paranthropus* and *Australopithecus* (Barak et al., 2013; DeSilva and Devlin, 2012; Macchiarelli et al., 1999; Su, 2011; Ryan et al., 2018; Su and Carlson, 2017; Su et al., 2013; Zeininger et al., 2016).

5. Conclusions

Patellar remains are rare in the hominin fossil record. In the comparative context considered in this study, the coupled signals from what is preserved and suitable for analysis of the outer morphology and inner structural arrangement of the early Pleistocene patella SKX 1084 from Swartkrans Member 2, South Africa, indicate that it belonged to an adult small-bodied hominin (Susman, 1989) likely equipped for exploiting a limited home range size (Ramirez and Pontzer, 2015). Its habitual postural- and locomotion-related charges at the knee joint appear compatible with, but not fully overlapping the human condition as represented by the late Pleistocene and Holocene comparative materials examined so far. When compared to what is currently known on the structural bony characteristics of the postcranial skeleton in fossil hominins, the inner features assessed in SKX 1084 (i.e. thickness of the cortical shell and cancellous bone textural properties) globally fit the general australopith pattern (cf. Ryan et al., 2018). In the absence of any signal from patellae unambiguously attributed to *Paranthropus*, as well as of comparable evidence extracted from specimens representing early *Homo*

(the patella D3418 from Dmanisi; Lordkipanidze et al., 2007), the attribution of SKX 1084 to the taxon *P. robustus* (Susman, 1988, 1989; Susman et al., 2001) cannot be rejected, and still represents a reasonable assessment.

Acknowledgements

For access to fossil and comparative materials, we are grateful to the curators of the Ditsong National Museum of Natural History, Pretoria; the Pretoria Bone Collection at the Department of Anatomy of the University of Pretoria; and the Evolutionary Studies Institute at the University of the Witwatersrand. For the realization at the ICTP Multidisciplinary Lab. of Trieste of scans of comparative human material stored at the National Museum "L. Pigorini" of Rome, we acknowledge F. Bernardini, L. Bondioli, C. Tuniz, and C. Zanolli; we also acknowledge M. Nakamura (Kyoto) and Y. Shintaku (Inuyama) for access to the *Pan* specimens used in this study. For their kind contribution during various analytical phases (including the intra- and inter-observer tests), we are especially grateful to A. Beaudet (Johannesburg) and C. Zanolli (Toulouse). For collaboration and discussion, we also thank L. Bam (Pelindaba), J. Braga (Toulouse & Johannesburg), L. Bruxelles (Toulouse and Johannesburg), R.J. Clarke (Johannesburg), J. Dumoncel (Toulouse), J. Heaton (Birmingham and Johannesburg), T. Jashashvili (Johannesburg), L. Kgasi (Pretoria), K. Kuman (Johannesburg), D. Marchi (Pisa), T. Pickering (Madison and Johannesburg), S. Potze (Pretoria), B. Zipfel (Johannesburg). The comments from two reviewers significantly enhanced the quality of the first version of this study. We acknowledge the DST-NRF for the financial support (Grant # UID23456) to establish the MIXRAD micro-focus X-ray tomography facility at Necsa. M.C. is funded by the European Commission (EACEA), Erasmus Mundus programme, AESOP and AESOP+ consortia coordinated by J. Braga (Toulouse).

Appendix A. Supplementary data

Supplementary data associated with this article can be found, in the online version, at https://doi.org.10.1016/j.crpv.2018.06.002.

References

Aglietti, P., Menchetti, P.P.M., 1995. Biomechanics of the patellofemoral joint. In: Scuderi, G.R. (Ed.), The patella. Springer, New York, pp. 25–48.

Aiello, L., Dean, C., 1990. An introduction to human evolutionary anatomy. Academic Press, New York.

Antón, S.C., 2013. *Homo erectus* and related taxa. In: Begun, D.R. (Ed.), A Companion to Paleoanthropology. Blackwell Publ, Chichester, UK, pp. 497–516.

Antón, S.C., Potts, R., Aiello, L.C., 2014. Evolution of early *Homo*: An integrated biological perspective. Science 345, 45–58.

Alemseged, Z., Spoor, F., Kimbel, W.H., Bobe, R., Geraads, D., Reed, D., Wynn, J.G., 2006. A juvenile early hominin skeleton from Dikika, Ethiopia. Nature 443, 296–301.

Baldwin, J.L., House, C.K., 2005. Anatomic dimensions of the patella measured during total knee arthroplasty. J. Arthroplasty 20, 250–257.

Balter, V., Blichert-Toft, J., Braga, J., Telouk, P., Thackeray, F., Albarède, F., 2008. U-Pb dating of fossil enamel from the Swartkrans Pleistocene hominid site, South Africa. Earth Planet. Sci. Lett. 267, 236–246.

Barak, M.M., Lieberman, D.E., Raichlen, D., Pontzer, H., Warrener, A.G., Hublin, J.-J., 2013. Trabecular evidence for a human-like gait in *Australopithecus africanus*. PLoS ONE 8, 1–9.

Bayle, P., Bondioli, L., Macchiarelli, R., Mazurier, A., Puymerail, L., Volpato, V., Zanolli, C., 2011. Three-dimensional imaging and quantitative characterization of human fossil remains. Examples from the NESPOS database. In: Macchiarelli, R., Weniger, G.-C. (Eds.), Pleistocene databases. Acquisition, storing, sharing. Wissenschaftliche Schriften des Neanderthal Museums 4, Mettmann, pp. 29–46.

Beauchesne, P., Agarwal, S.C., 2017. A multi-method assessment of bone maintenance and loss in an Imperial Roman population: Implications for future studies of age-related bone loss in the past. Am. J. Phys. Anthropol 164, 41–61.

Beaudet, A., Bernardini, F., Cazenave, M., Mazurier, A., Radovčić, D., Radovčić, J., Tuniz, C., Volpato, V., Macchiarelli, R., 2013. The Neanderthal patella: Topographic bone distribution and inner structural organization. Proc. Europ. Soc. Study Hum. Evol. 2, 41.

Berger, L.R., de Ruiter, D.J., Churchill, S.E., Schmid, P., Carlson, K.J., Dirks, P.H.G.M., Kibii, J.M., 2010. *Australopithecus sediba*: A new species of *Homo*-like australopith from South Africa. Science 328, 195–204.

Berger, L.R., Hawks, J., de Ruiter, D.J., Churchill, S.E., Schmid, P., Delezene, L.K., Kivell, T.L., Garvin, H.M., Williams, S.A., DeSilva, J.M., Skinner, M.M., Musiba, C.M., Cameron, N., Holliday, T.W., Harcourt-Smith, W., Ackermann, R.R., Bastir, M., Bogin, B., Bolter, D., Brophy, J., Cofran, Z.D., Congdon, K.A., Deane, A.S., Dembo, M., Drapeau, M., Elliott, M.C., Feuerriegel, E.M., Garcia-Martinez, D., Green, D.J., Gurtov Al, Irish, J.D., Kruger, A., Laird, M.F., Marchi, D., Meyer, M.R., Nalla, S., Negash, E.W., Orr, C.M., Radovcic, D., Schroeder, L., Scott, J.E., Throckmorton, Z., Tocheri, M.W., VanSickle, C., Walker, C.S., Wei, P., Zipfel, B., 2015. *Homo naledi*, a new species of the genus *Homo* from the Dinaledi Chamber, South Africa. eLife 4, 1–35.

Bleuze, M.M., 2010. Cross-sectional morphology and mechanical loading in Plio-Pleistocene hominins: Implications for locomotion and taxonomy. PhD dissertation. The University of Western Ontario, Ontario.

Bookstein, F.L., 1991. Morphometric tools for landmark data: Geometry and biology. Cambridge University Press, Cambridge, UK.

Braga, J., Fourvel, J.-B., Lans, B., Bruxelles, L., Thackeray, J.F., 2016. The Kromdraai hominins revised with an updated portrayal of differences between *Australopithecus africanus* and *Paranthropus robustu*. In: Braga, J., Thackeray, J.F. (Eds.), Kromdraai, a birthplace of *Paranthropus*in the Cradle of Humankind. Sun Press, Johannesburg, pp. 49–68.

Carlson, K.J., Marchi, D., 2014. Reconstructing mobility. Environmental, behavioral and morphological determinants. Springer, New York.

Carretero, J.M., Lorenzo, C., Arsuaga, J.L., 1999. Axial and appendicular skeleton of *Homo antecessor*. J. Hum. Evol. 37, 459–499.

Carretero, J.M., Lorenzo, C., Arsuaga, J.L., 2001. Restes post-crâniens du niveau TD6 du site en grotte du Pléistocène inférieur de Gran Dolina, Sierra de Atapuerca, Espagne. Anthropologie 105, 179–202.

Cazenave, M., Beaudet, A., Braga, J., Oettlé, A., Thackeray, J.F., Hoffman, J., de Beer, F., Macchiarelli, R., 2016. The inner structural organization of a (likely) paranthropine patella from Swartkrans Member 2 (SKX 1084): Human- and nonhuman-like features. Am. J. Phys. Anthropol. 159 (Suppl. 62), 111–112.

Cazenave, M., Braga, J., Oettlé, A., Thackeray, J.F., de Beer, F., Hoffman, J., Endalamaw, M., Redae, B.E., Puymerail, L., Macchiarelli, R., 2017. Inner structural organization of the distal humerus in *Paranthropus* and *Homo*. In: Macchiarelli, R., Zanolli, C. (Eds.), Hominin biomechanics, virtual anatomy and inner structural morphology: From head to toe. A tribute to Laurent Puymerail. C. R. Palevol, 16, pp. 521–532.

Chirchir, H., Kivell, T.L., Ruff, C.B., Hublin, J.-J., Carlson, K.J., Zipfel, B., Richmond, B.G., 2015. Recent origin of low trabecular bone density in modern humans. Proc. Natl. Acad. Sci. USA. 112, 366–371.

Chirchir, H., Ruff, C.B., Junno, J.A., Potts, R., 2017. Low trabecular bone density in recent sedentary modern humans. Am. J. Phys. Anthropol. 162, 550–560.

Coleman, M.N., Colbert, M.W., 2007. Technical note: CT thresholding protocols for taking measurements on three-dimensional models. Am. J. Phys. Anthropol. 133, 723–725.

Dalstra, M., Huiskes, R., 1995. Load transfer across the pelvic bone. J. Biomech 28, 715–724.

Dayal, M.R., Bidmos, A.B., 2005. Discriminating sex in South African blacks using patella dimensions. J. Forensic Sci. 50, JFS2004306–JFS2004314.

Dean, M.C., Wood, B.A., 2003. A digital radiographic atlas of great ape skull and dentition. In: Bondioli, L., Macchiarelli, R. (Eds.), Digital archives of human paleobiology. 3. Museo Nazionale "L. Pigorini", Rome.

Delson, E., 1988. Chronology of South African australopith site units. In: Grine, F.E. (Ed.), Evolutionary history of the "robust" australopithecines. Aldine de Gruyter, New York, pp. 317–324.

DeSilva, J.M., Devlin, M.J., 2012. A comparative study of the trabecular bony architecture of the talus in humans, non-human primates, and *Australopithecus*. J. Hum. Evol. 63, 536–551.
DeSilva, J.M., Holt, K.G., Churchill, S.E., Carlson, K.J., Walker, C.S., Zipfel, B., Berger, L.R., 2013. The lower limb and mechanics of walking in *Australopithecus sediba*. Science 340, 54–78.
Domínguez-Rodrigo, M., Pickering, T.R., Baquedano, E., Mabulla, A., Mark, D.F., Musiba, C., Pérez-González, A., 2013. First partial skeleton of a 1.34-million-year-old *Paranthropus boisei* from Bed II, Olduvai Gorge, Tanzania. PLoS ONE 8, e80347.
Dowdeswell, M.R., Jashashvili, T., Patel, B.A., Lebrun, R., Susman, R.L., Lordkipanidze, D., Carlson, K.J., 2016. Adaptation to bipedal gait and fifth metatarsal structural properties in *Australopithecus*, *Paranthropus*, and *Homo*. In: Macchiarelli, R., Zanolli, C. (Eds.), Hominin biomechanics, virtual anatomy and inner structural morphology: From head to toe. A tribute to Laurent Puymerail. C. R. Palevol, 16, pp. 585–599.
Fajardo, R.J., Ryan, T.M., Kappelman, J., 2002. Assessing the accuracy of high-resolution X-ray computed tomography of primate trabecular bone by comparisons with histological sections. Am. J. Phys. Anthropol. 118, 1–10.
Frelat, M.A., Shaw, C.N., Sukhdeo, S., Hublin, J.-J., Benazzi, S., Ryan, T.M., 2017. Evolution of the hominin knee and ankle. J. Hum. Evol. 108, 147–160.
Gibbon, R.J., Pickering, T.R., Sutton, M.B., Heaton, J.L., Kuman, K., Clarke, R.J., Brain, C.K., Granger, D.E., 2014. Cosmogenic nuclide burial dating of hominin-bearing Pleistocene cave deposits at Swartkrans, South Africa. Quat. Geochron. 24, 10–15.
Goodfellow, J., Hungerford, D.S., Zindel, M., 1976. Patello-femoral joint mechanics and pathology. J. Bone Joint Surg. 58, 287–290.
Gosman, J.H., Stout, S.D., Larsen, C.S., 2011. Skeletal biology over the life span: A view from the surfaces. Am. J. Phys. Anthropol. 146, 86–98.
Grine, F.E., Susman, R.L., 1991. Radius of *Paranthropus robustus* from Member 1, Swartkrans Formation, South Africa. Am. J. Phys. Anthropol. 84, 229–248.
Harrison, T., Kweka, A., 2011. Paleontological localities on the Eyasi Plateau including Laetoli. In: Harrison, T. (Ed.), Paleontology and geology of Laetoli: Human evolution in context: volume 1: geology, geochronology, paleoecology and paleoenvironment. Springer, Dordrecht, pp. 17–45.
Herries, A.I.R., Curnoe, D., Adams, J.W., 2009. A multi-disciplinary seriation of early *Homo* and *Paranthropus* bearing palaeocaves in southern Africa. Quat. Int. 202, 14–28.
Huiskes, R., 2000. If bone is the answer, then what is the question? J. Anat. 197, 145–156.
Iranpour, F., Merican, A.M., Amis, A.A., Cobb, J.P., 2008. The width: Thickness ratio of the patella. Clin. Orthop. Related Res. 466, 1198–1203.
Jungers, W.L., 1988. New estimates of body size in australopithecines. In: Grine, F.E. (Ed.), The evolutionary history of the "robust" australopithecines. Aldine de Gruyter, New York, pp. 115–125.
Jungers, W.L., Larson, S.G., Harcourt-Smith, W., Morwood, M.J., Sutikna, T., Awe, R.D., Djubiantono, T., 2009. Descriptions of the lower limb skeleton of *Homo floresiensis*. J. Hum. Evol. 57, 538–554.
Katoh, T., Griffin, M.P., Wevers, H.W., Rudan, J., 1996. Bone hardness testing in the trabecular bone of the human patella. J. Arthroplasty 11, 460–468.
Kemkes-Grottenthaler, A., 2005. Sex determination by discriminant analysis: an evaluation of the reliability of patella measurements. Forensic Sci. Int. 147, 129–133.
Keyser, A., Menter, C.G., Moggi-Cecchi, J., Pickering, T.R., Berger, L.R., 2000. Drimol: A new hominid-bearing site in Gauteng, South Africa. South Afr. J. Sci. 96, 193–197.
Kivell, T.L., 2016. A review of trabecular bone functional adaptation: What have we learned from trabecular analyses in extant hominoids and what can we apply to fossils? J. Anat. 228, 569–594.
L'Abbé, E.N., Loots, M., Meiring, J.H., 2005. The Pretoria bone collection: A modern South African skeletal sample. Homo 56, 197–205.
Lague, M.R., 2015. Taxonomic identification of Lower Pleistocene fossil hominins based on distal humeral diaphyseal cross-sectional shape. PeerJ 3, e1084.
Lieberman, D.E., Polk, J.D., Demes, B., 2004. Predicting long bone loading from cross-sectional geometry. Am. J. Phys. Anthropol. 123, 156–171.
Lordkipanidze, D., Jashashvili, T., Vekua, V., Ponce de Leon, M.S., Zollikofer, C.P.E., Rightmire, G.P., Pontzer, H., Ferring, R., Oms, O., Tappen, M., Bukhsianidze, M., Agusti, J., Kahlke, R., Kiladze, G., Martinez-Navarro, B., Mouskhelishvili, A., Nioradze, M., Rook, L., 2007. Postcranial evidence from early *Homo* from Dmanisi, Georgia. Nature 449, 305–310.
Lovejoy, C.O., 2007. The natural history of human gait and posture: Part 3. The knee. Gait & Post 25, 325–341.
Macchiarelli, R., Bondioli, L., Galichon, V., Tobias, P.V., 1999. Hip bone trabecular architecture shows uniquely distinctive locomotor behaviour in South African australopithecines. J. Hum. Evol. 36, 211–232.
Macchiarelli, R., Rook, L., Bondioli, L., 2001. Comparative analysis of the iliac trabecular architecture in extant and fossil primates by means of digital image processing techniques: Implications for the reconstruction of fossil locomotor behaviours. In: de Bonis, L., Koufos, G., Andrews, P. (Eds.), Hominoid evolution and climatic change in Europe. Vol. 2. Phylogeny of the Neogene hominoid primates of Eurasia. Cambridge University Press, Cambridge, UK, pp. 60–101.
Marchi, D., Walker, C.S., Wei, P., Holliday, T.W., Churchill, S.E., Berger, L.R., DeSilva, J.M., 2017. The thigh and leg of *Homo naledi*. J. Hum. Evol. 104, 174–204.
Mariani, P.P., Puddu, G., Ferretti, A., 1978. Jumper's knee. Ital. J. Orthopaed. Traumat. 4, 85–93.
Martín-Francés, L., Martinón-Torres, M., Gracia-Téllez, A., Bermúdez de Castro, J.M., 2016. Evidence of trauma in a ca. 1-million-year-old patella of *Homo* antecessor, Gran Dolina-Atapuerca (Spain). C. R. Palevol 15, 1011–1016.
Masouros, S.D., Bull, A.M.J., Amis, A.A., 2010. Biomechanics of the knee joint. Orthopaed. Trauma 24, 84–91.
Maureille, B., Gómez-Olivencia, A., Couture-Veschambre, C., Madelaine, S., Holliday, T., 2015. Nouveaux restes humains provenant du gisement de Regourdou (Montignac-sur-Vézère, Dordogne, France). Paleo 26, 117–138.
Mazurier, A., 2006. Relations entre comportement locomoteur et variation cortico-trabéculaire du plateau tibial chez les Primates: analyse quantitative non invasive à haute résolution (SR-μCT) et applications au registre fossile. PhD dissertation. Université de Poitiers, Poitiers, France.
Mazurier, A., Nakatsukasa, M., Macchiarelli, R., 2010. The inner structural variation of the primate tibial plateau characterized by high-resolution microtomography. Implications for the reconstruction of fossil locomotor behaviours. C. R. Palevol 9, 349–359.
Mazurier, A., Volpato, V., Macchiarelli, R., 2006. Improved noninvasive microstructural analysis of fossil tissues by means of SR-microtomography. Appl. Phys. A. Mat. Sci. Process. 83, 229–233.
McHenry, H.M., 1975. A new pelvic fragment from Swartkrans and the relationship between the robust and gracile australopithecines. Am. J. Phys. Anthropol. 43, 245–262.
McHenry, H.M., 1991. Petite bodies of the "robust" australopithecines. Am. J. Phys. Anthropol. 86, 445–454.
McHenry, H.M., Brown, C.C., McHenry, L.J., 2007. Fossil hominin ulnae and the forelimb of *Paranthropus*. Am. J. Phys. Anthropol. 134, 209–218.
Mitteroecker, P., Bookstein, F.L., 2011. Linear discrimination, ordination, and the visualization of selection gradients in modern morphometrics. Evol. Biol. 38, 100–114.
Mitteroecker, P., Gunz, P., Windhager, S., Schaefer, K., 2013. A brief review of shape, form, and allometry in geometric morphometrics, with applications to human facial morphology. Hystrix 24, 59–66.
Moggi-Cecchi, J., Menter, C., Boccone, S., Keyser, A., 2010. Early hominid dental remains from the Plio-Pleistocene site of Drimolen, South Africa. J. Hum. Evol. 58, 374–405.
Olateju, O.I., Philander, I., Bidmos, M.A., 2013. Morphometric analysis of the patella and patellar ligament of South Africans of European ancestry. South Afr. J. Sc. 109, 1–6.
Pearson, O.M., Lieberman, D.E., 2004. The aging of Wolff's law: Ontogeny and responses to mechanical loading in cortical bone. Yearb. Phys. Anthropol. 47, 63–99.
Pickering, T.R., Heaton, J.L., Clarke, R.J., Sutton, M.B., Brain, C.K., Kuman, K., 2012. New hominid fossils from Member 1 of the Swartkrans formation, South Africa. J. Hum. Evol 62, 618–628.
Pina, M., 2016. Unravelling the positional behaviour of fossil hominoids: Morphofunctional and structural analysis of the primate hindlimb. PhD dissertation. Universidad Autònoma de Barcelona, Barcelona, Spain.
Pina, M., Almécija, S., Alba, D.M., O'Neill, M.C., Moyà-Solà, S., 2014. The middle Miocene ape *Pierolapithecus catalaunicus* exhibits extant great ape-like morphometric affinities on its patella: Inferences on knee function and evolution. PLoS One 9, e91944.
Pritchard, J.L., 1980. An osteometric analysis of the patella and femur in *Pan*, *Gorilla* and *Homo*. PhD dissertation. School of The Ohio State University, Colombus, OH, USA.
R Development Core Team, 2017. R: A Language and Environment for Statistical Computing, Available at: http://www.R-project.org.
Radovčić, J., Smith, F.H., Trinkaus, E., Wolpoff, M.H., 1988. The Krapina hominids. An illustrated catalog of skeletal collection. Croatian Natural History Museum, Zagreb.

Ramirez, K.R., Pontzer, H., 2015. Estimates of fossil hominin quadriceps physiological cross sectional area from patellar dimensions. Am. J. Phys. Anthropol. 156, 261.
Raux, P., Townsend, P.R., Miegel, R., Rose, R.M., Radin, E.L., 1975. Trabecular architecture of the human. J. Biomech. 8, 1–17.
Ruff, C.B., Higgins, R., 2013. Femoral neck structure and function in early hominins. Am. J. Phys. Anthropol. 150, 512–525.
Ruff, C.B., Holt, B., Trinkaus, E., 2006. Who's afraid of the big bad Wolff?: Wolff's law and bone functional adaptation. Am. J. Phys. Anthropol. 129, 484–498.
Ruff, C.B., McHenry, H.M., Thackeray, J.F., 1999. Cross-sectional morphology of the SK 82 and 97 proximal femora. Am. J. Phys. Anthropol. 109, 509–521.
Ryan, T.M., Ketcham, R., 2002a. The three-dimensional structure of trabecular bone in the femoral head of strepsirrhine primates. J. Hum. Evol. 43, 1–26.
Ryan, T.M., Ketcham, R., 2002b. Femoral head trabecular bone structure in two omomyid primates. J. Hum. Evol. 43, 241–263.
Ryan, T.M., Shaw, C.N., 2015. Gracility of the modern *Homo sapiens* skeleton is the result of decreased biomechanical loading. Proc. Natl. Acad. Sci. USA 112, 372–377.
Ryan, T.M., Walker, A., 2010. Trabecular bone structure in the humeral and femoral heads of anthropoid primates. Anat. Rec. 293, 719–729.
Ryan, T.M., Carlson, K.J., Gordon, A.D., Jablonski, N., Shaw, C.N., Stock, J.T., 2018. Human-like hip joint loading in *Australopithecus africanus* and *Paranthropus robustus*. J. Hum. Evol., http://dx.doi.org/10.1016/j.jhevol.2018.03.008.
Schlager, S., 2017. Morpho: Calculations and visualizations related to geometric morphometrics. R package version 2.5., pp. 1.
Schneider, C.A., Rasband, W.S., Eliceiri, K.W., 2012. NIH Image to ImageJ: 25 years of image analysis. Nature Meth. 9, 671–675.
Schwartz, J.H., Tattersall, I., 2003. The Human fossil record. Vol. 2. Craniodental morphology of genus *Homo* (Africa and Asia). Wiley-Liss, New York.
Shaw, C., Ryan, T., 2012. Does skeletal anatomy reflect adaptation to locomotor patterns? Cortical and trabecular architecture in human and nonhuman anthropoids. Am. J. Phys. Anthropol. 147, 187–200.
Skinner, M.M., Stephens, N.B., Tsegai, Z.J., Foote, A.C., Nguyen, N.H., Gross, T., Pahr, D.H., Hublin, J., Kivell, T.L., 2015. Human-like hand use in *Australopithecus africanus*. Science 347, 395–399.
Spoor, F., Zonneveld, F., Macho, G., 1993. Linear measurements of cortical bone and dental enamel by computed tomography: applications and problems. Am. J. Phys. Anthropol. 91, 469–484.
Standring, S., 2008. Gray's anatomy: The anatomical basis of clinical practice. Elsevier Health Sciences, UK.
Su, A., 2011. The functional morphology of subchondral and trabecular bone in the hominoid tibiotalar joint. PhD dissertation. Stony Brook University, New York.
Su, A., Carlson, K.J., 2017. Comparative analysis of trabecular bone structure and orientation in South African hominin tali. J. Hum. Evol. 106, 1–18.
Su, A., Wallace, I.J., Nakatsukasa, M., 2013. Trabecular bone anisotropy and orientation in an early Pleistocene hominin talus from East Turkana, Kenya. J. Hum. Evol. 64, 667–677.
Susman, R.L., 1988. New postcranial remains from Swartkrans and their bearing on the functional morphology and behavior of *Paranthropus robustus*. In: Grine, F.E. (Ed.), The evolutionary history of the "robust" australopithecines. Aldine de Gruyter, New York, pp. 149–172.
Susman, R.L., 1989. New hominid fossils from the Swartkrans formation (1979-1986 excavations): Craniodental specimens. Am. J. Phys. Anthropol. 79, 451–474.
Susman, R.L., 2004. Swartkrans; a cave's chronicle of early man. Hominid postcranial remains from Swartkrans. Transv. Mus. Monogr. 8 (Pretoria).
Susman, R.L., Brain, T.M., 1988. New first metatarsal (SKX 5017) from Swartkrans and the gait of *Paranthropus robustus*. Am. J. Phys. Anthropol. 77, 7–15.
Susman, R.L., de Ruiter, D.J., 2004. New hominin first metatarsal (SK 1813) from Swartkrans. J. Hum. Evol. 47, 171–181.
Susman, R.L., de Ruiter, D., Brain, C.K., 2001. Recently identified postcranial remains of *Paranthropus* and early *Homo* from Swartkrans Cave, South Africa. J. Hum. Evol. 41, 607–629.
Sylvester, A., 2013. A geometric morphometric analysis of the medial tibial condyle of African hominids. Anat. Rec. 296, 1518–1525.
Sylvester, A.D., Mahfouz, M.R., Kramer, P.A., 2011. The effective mechanical advantage of AL 129-1a for knee extension. Anat. Rec. 294, 1486–1499.
Tardieu, C., 1999. Ontogeny and phylogeny of femoro-tibial characters in humans and hominid fossils: Functional influence and genetic determinism. Am. J. Phys. Anthropol. 110, 365–377.
Taylor, W.R., Heller, M.O., Bergmann, G., Duda, G.N., 2004. Tibio-femoral loading during human gait and stair climbing. J. Orthop. Res. 22, 625–632.
Toumi, H., Higashiyama, I., Suzuki, D., Kumai, T., Bydder, G., McGonagle, D.D., Emery, P., Fairclough, J., Benjamin, M., 2006. Regional variations in human patellar trabecular architecture and the structure of the proximal patellar tendon enthesis. J. Anat. 208, 47–57.
Toumi, H., Larguech, G., Filaire, E., Pinti, A., Lespessailles, E., 2012. Regional variations in human patellar trabecular architecture and the structure of the quadriceps enthesis: A cadaveric study. J. Anat. 220, 632–637.
Touraine, S., Bouhadoun, H., Engelke, K., Laredo, J.D., Chappard, C., 2017. Influence of meniscus on cartilage and subchondral bone features of knees from older individuals: A cadaver study. PLoS ONE 12, e0181956.
Townsend, P.R., Raux, P., Rose, R.M., Miegel, R.E., Radin, E.L., 1975. The distribution and anisotropy of the stiffness of cancellous bone in the human patella. J. Biomech. 8, 363–367.
Townsend, P.R., Rose, R.M., Radin, E.L., Raux, P., 1977. The biomechanics of the human patella and its implications for chondromalacia. J. Biomech. 10, 403–407.
Trinkaus, E., 1983. The Shanidar Neandertals. Academic Press, New York.
Tuniz, C., Bernardini, F., Cicuttin, A., Crespo, M.L., Dreossi, D., Gianoncelli, A., Mancini, L., Mendoza Cuevas, A., Sodini, N., Tromba, G., Zanini, F., Zanolli, C., 2013. The ICTP-Elettra X-ray laboratory for cultural heritage and archaeology. Nucl. Instr. Meth. Phys. Res. A: Acceler., Spectrom., Detect. Ass. Equipm. 711, 106–110.
Vandermeersch, B., 1981. Les hommes fossiles de Qafzeh (Israël). CNRS, Paris.
Volpato, V., 2007. Morphogenèse des propriétés texturales du tissu osseux et environnement biomécanique. Caractérisation non invasive du réseau trabéculaire et de l'os cortical du squelette appendiculaire de mammifères actuels et fossiles, hominidés inclus. PhD dissertation. Université de Poitiers, Poitiers, France.
Vrba, E.S., 1975. Some evidence of chronology and palaeoecology of Sterkfontein, Swartkrans and Kromdraai from the fossil Bovidae. Nature 254, 301–304.
Wallace, I.J., Tommasini, S.M., Judex, S., Garland Jr., T., Demes, B., 2012. Genetic variations and physical activity as determinants of limb bone morphology: An experimental approach using a mouse model. Am. J. Phys. Anthropol. 148, 24–35.
Ward, C.V., Ruff, C.B., Walker, A., Teaford, M.F., Rose, M.D., Nengo, I.O., 1995. Functional morphology of Proconsul patellas from Rusinga Island, Kenya, with implications for other Miocene–Pliocene catarrhines. J. Hum. Evol. 29, 1–19.
Yoo, J.H., Yi, S.R., Kim, J.H., 2007. The geometry of patella and patellar tendon measured on knee MRI. Surg. Rad. Anat. 29, 623–666.
Zeininger, A., Patel, B.A., Zipfel, B., Carlson, K.J., 2016. Trabecular architecture in the StW 352 fossil hominin calcaneus. J. Hum. Evol. 97, 145–158.
Zeininger, A., Richmond, B.G., Hartman, G., 2011. Metacarpal head biomechanics: A comparative backscattered electron image analysis of trabecular bone mineral density in Pan troglodytes, *Pongo pygmaeus*, and *Homo sapiens*. J. Hum. Evol. 60, 703–710.
Zipfel, B., Berger, L.R., 2009. Partial hominin tibia (StW 396) from Sterkfontein, South Africa. Palaeont. Afr. 44, 71–75.